

## Development of Affordable and Compact Muon Tomography Detector

---

**Shih-Chieh Su,\* Ying-Chih Chen, Jiwoo Nam, Pisin Chen, and Chung-Yun Kuo**

*<sup>a</sup>Department of Physics and Leung Center for Cosmology and Particle Astrophysics, National Taiwan University, No. 1, Sec. 4, Roosevelt Rd., Taipei 10617, Taiwan*

*E-mail: [jackysu822@gmail.com](mailto:jackysu822@gmail.com)*

Geiger–Müller Muon Telescope in Taiwan (GMT<sup>2</sup>) is an education program for undergraduate students to develop a muon tomography detector composed of Geiger–Müller (GM) tubes. GMT<sup>2</sup> consists of two identical detector plates aligned on an axis at a distance. Each detector plate contains two orthogonal 1-D arrays of 8 GM tubes ( $L=18$  cm,  $\phi=2.2$  cm), forming an  $8 \times 8$  grid. The arrival direction of muons can be reconstructed by extrapolating the impact points recorded on two detector plates. Field of view (FOV) of GMT<sup>2</sup> is adjustable by varying the distance between two detector plates. Small size and low unit price of GM tubes make GMT<sup>2</sup> affordable (US\$700) and compact ( $40 \times 40 \times 40$  cm<sup>3</sup>). Several muon tomography experiments were successfully carried out for buildings, such as C.C. Leung Cosmology Hall, National Taiwan University and Taipei 101. In this paper, we report details of system design, detector construction, data acquisition, data analysis, and results.

38<sup>th</sup> International Cosmic Ray Conference (ICRC 2023)  
July 26th – Aug 3rd, 2023  
Nagoya, Japan



---

\*Speaker

## 1. Introduction

Muon tomography is an emerging technique that generates 2-D or 3-D density maps of dense objects utilizing excellent penetrating power and abundant flux of cosmic muons. In recent years, several successful experiments have demonstrated the potential of muon tomography in investigating hidden large structures, including the discovery of a hidden chamber within the Khufu pyramid [1] and the identification of lava chambers within the La Soufriere Volcano [2].

Muon tomography is also an intriguing educational subject due to its intuitiveness and simplicity of the method. Results obtained with the internal density distribution of the objects can be highly visualized, providing a compelling incentive and commanding students' keen interest. In this paper, we report the development of an educational muon tomography detector using Geiger-Müller (GM) tubes. The main considerations in detector design are as follows: 1) The system should be simple enough for undergraduate students to build it themselves. 2) It should be compact, portable, and automotive, allowing easy experimentation in various locations. 3) The manufacturing cost should be affordable, enabling the project to be carried out within the educational budget of schools. 4) The time required for detector fabrication and experimentation should range from a few months to within one year, ensuring completion within an academic year. This program enables student participation in every aspect of the experimental process, including detector design, fabrication, data taking, data analysis, and simulation.

Our muon tomography detector, named as Geiger Müller muon Telescope in Taiwan (GMT<sup>2</sup>), consists of two detection plates, providing a pair of x-y impact points per muon. By extrapolating these paired points, we obtain the arrival direction of the incoming muon. The distance between the detection plates is adjustable, providing the flexibility to adjust the field of view (FOV) according to the target being observed. Each detection plate consists of two layers of GM tube arrays, with eight GM tubes arranged in parallel in each layer. By placing these two layers orthogonally to each other, we have implemented an  $8 \times 8$  x-y grid for obtaining impact point. Using GM tubes, which have a simple and stable operation and are cost-effective, to implement this muon tomography detector meets our requirements exceptionally well. With commercial GM tubes measuring 22mm in diameter and 180mm in length, we have implemented a 180mm  $\times$  180mm detection plate. With a distance of 200 mm between the two detection plates, an FOV of  $90^\circ \times 90^\circ$  is achieved. While it is a drawback that this method does not work for multi-muon events, the probability of multi-muon occurrences within the size of our detector is not significantly high. Designing a high-voltage power supply capable of driving a total of 32 GM tubes, each operating at 400V, presented one of the most formidable challenges in our project. To overcome this, we engineered a cost-effective high voltage supply by leveraging cold cathode fluorescent lamp (CCFL) inverters with a rectifier circuit.

In the following sections, we present a detailed design of the GMT<sup>2</sup> and experimental results for two observation objects to demonstrate the feasibility of our approach.

## 2. Instrument Design

### 2.1 High voltage supply

Our GM tubes require a working voltage of 400V. To provide the necessary high voltage for driving the GM tubes, we employ a CCFL inverter. This CCFL inverter, in conjunction with

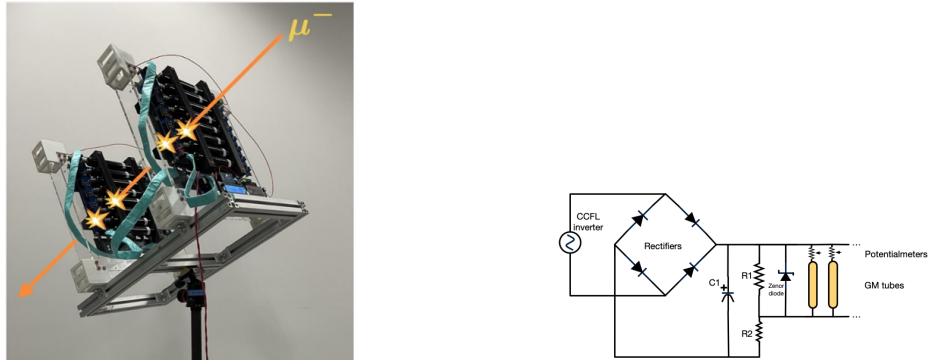


Figure 1: (Left) GMT<sup>2</sup> detector. (Right) A circuit schematic diagram for the HV module.

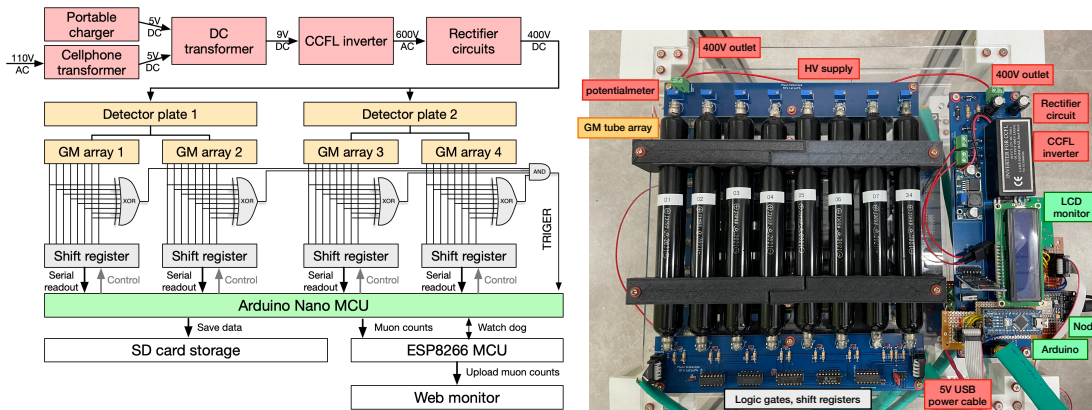


Figure 2: (Left) A system schematic diagram. Power modules is colored in red, GM tubes are colored in orange, ICs are colored in grey and Data acquisition modules are colored in green. (Right) The first layer of GMT<sup>2</sup>. The power rectification circuit and MCUs are integrated in a PCB located on the first layer. The GM tube array is hold by a HV supply board and a signal processing board on each layer.

a rectifier circuit (Fig. 1(R)), converts the 5V input from the USB port into 400V, ensuring a consistent power supply for the parallel operation of 32 GM tubes. This integration of the CCFL inverter offers a cost-effective and compact solution for high voltage supply.

The power consumption of the CCFL inverter stands at approximately 0.5 Watt, with each GM tube drawing a current of less than 10  $\mu$ A during electron avalanche. Consequently, the entire system’s power consumption is only 1.5 Watts, inclusive of the Arduino MCU’s consumption. This minimal power requirement, coupled with the convenience of the 5V USB power input, renders the GMT<sup>2</sup> system portable and self-contained and makes it suitable for operations in remote areas using portable chargers.

## 2.2 Triggers

When particles are detected by the GM tubes, the analog pulse signals undergo an initial digitization process, which converts them into square waves using inverters. These digitized signals are then directed to the shift registers. Simultaneously, the signals in each layer are fed into XOR gates, ensuring that only one tube within a layer is sending the signal, which rejects any double hits. The XOR outputs from each layer are subsequently routed to an AND gate for multi-layer

coincidence. This multi-layer coincidence triggers the Arduino MCU, which then proceeds to read the data from the shift registers. This approach enables the rapid filtering of events that cannot be reconstructed, such as electron events.

A typical pulse from the GM tubes lasts approximately  $300 \mu s$ , during which the trigger circuit is engaged, resulting in a dead time. However, due to the device's small effective area, the likelihood of a second pulse occurring during this dead time is minimal.

### 2.3 Data acquisition

Once triggered, the Arduino reads and processes the data from the shift registers. It then filters out events that cannot be reconstructed, and saves the remaining valid events to an SD card. The events that fall into the unreconstructable category, which account for approximately 10% of the total events, often encounter a double-hit issue within the same layer. This occurrence may arise from cross-talk effects during signal transmission over a distance of 1 meter.

Furthermore, an additional MCU is incorporated to establish a web monitor and a watchdog system, ensuring long-term experimentation. This MCU grants Wi-Fi accessibility and monitors the Arduino's operations by collecting and uploading the trigger rates to the web monitor. Should any malfunctions occur within the Arduino, the MCU takes proactive measures to initiate an automatic reboot.

## 3. Experiments

### 3.1 Chee-Chun Leung Cosmology Hall (CCLCH) experiment

The first muon tomography experiment was conducted within the CCLCH building, which also serves as the site of our research center. The building features a large cylindrical hollow with a diameter of 12 meters at the center and spans across eight floors. Its symmetrical structure along the North-South and East-West axes makes it an ideal subject for verifying the feasibility of GMT<sup>2</sup>. Our objective is to observe the inner structure of the CCLCH building.

To accomplish this, GMT<sup>2</sup> needed exposure to the muons penetrating the building, and this constitutes the attenuated muon flux. This was carried out at the B1 auditorium of the CCLCH building, with GMT<sup>2</sup> positioned at the center of the building and oriented towards the zenith. Then, we conducted observations of the background muon flux towards the zenith on the rooftop of the CCLCH building (refer to Figure 3(L)). A total of 16 days of data were collected for the attenuated muon flux, while 25 days of data were collected for the background muon flux.

### 3.2 Taipei 101 experiment

The iconic Taipei 101 skyscraper, once holding the record for the world's tallest building, has been chosen as the next target for muon tomography imaging. The objective is to capture the outline of Taipei 101 in the resulting images. Xinyi Elementary School was chosen as the experimental site due to its ideal viewing angle and close proximity to Taipei 101 after we visited and evaluated various candidate sites.

At Xinyi Elementary School, GMT<sup>2</sup> was positioned in an empty classroom to capture attenuated muon flux of Taipei 101. It was oriented towards the skyscraper at an azimuthal angle of N30°E and

an elevation angle of  $45^\circ$ . This configuration maximizes muon penetration through Taipei 101's structure. The data collection spanned approximately three weeks for two different FOV settings:  $90^\circ$  and  $66^\circ$ . Later, GMT<sup>2</sup> was relocated to an empty classroom at CCLCH while maintaining the same orientation and FOVs as in Xinyi Elementary School, in order to capture the background muon flux from the open sky (refer to Figure 3(R)). To enhance statistical reliability, the data collection period was extended to 95 days for the  $90^\circ$  FOV and 132 days for the  $66^\circ$  FOV.

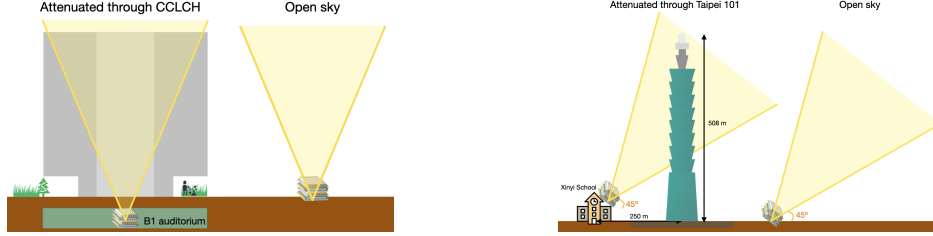


**Figure 3:** Schematic diagrams of the apparatus setup for (Left) CCLCH; (Right) Taipei 101 muon tomography image exposure.

### 3.3 Data analysis

In our muon tomography methodology, we calculate material lengths within the field of view to generate 2-D density maps, which are then displayed in our images. To measure the length for certain materials along specific directions, we apply the absorption method to muons arriving from those directions.

This is accomplished by comparing the attenuated muon flux, denoted as  $F_f(\theta, \varphi)$ , with the background muon flux, denoted as  $F_i(\theta, \varphi)$ , where  $(\theta, \varphi)$  represents the zenith and azimuth angles of the incoming direction. The ratio between them,  $F_f/F_i$ , signifies the muon survival rate and provides information about the interaction depth. The interaction depth for the specific incoming direction can be determined using Equation 1 and subsequently converted into material length, assuming we have prior knowledge of the material's density.

$$\frac{F_f(\theta, \varphi)}{F_i(\theta, \varphi)} = \exp\left(-\frac{\rho d}{\lambda}\right), \quad (1)$$

where  $\lambda$  is the muon attenuation depth,  $1030 \text{ g/cm}^2$  [3] for 4 GeV muons [4] reaching sea-level,  $\rho$  is density of the material in interest, and  $d$  is the thickness of the material along the muon trajectory at a given angle. The product of  $\rho$  and  $d$  gives us the interaction depth of certain material along the specific direction.

In this study, we computed the ratio between the attenuated muon flux that traversed the buildings and the background muon flux originating from the open sky. This ratio was then transformed into effective concrete length, assuming the presence of RC concrete ( $\rho = 2.4 \text{ g/cm}^3$  [5]) in the buildings, leading to muon attenuation. These effective concrete lengths corresponding to the 2-D density distribution map of the objects are presented in our muon tomography images.

### 3.4 Simulation

We employed the Cern ROOT program to simulate expected muon tomography images for the observed buildings. Within the program, we created models of the buildings under observation

— namely, CCLCH and Taipei 101. The simulated GMT<sup>2</sup> device was positioned and oriented to match its counterpart in each real-world experiment. During the modeling process, we focused on representing the RC (Reinforced Concrete) framework of the buildings, referring to engineering drawings[5], and ignore other structures or materials for simplicity.

Within the simulation, we generated ten million muon rays, each with randomized positions and incoming directions. For each muon ray that intersected with the GMT<sup>2</sup> apparatus, we calculated the length of concrete along its trajectory, and recorded this information in the corresponding bin of the expected muon tomography image for its incoming direction.

By comparing these expected muon tomography images with the data collected during the real-world experiments, we can validate the feasibility of GMT<sup>2</sup> and assess the level of error present in such long-term observations.

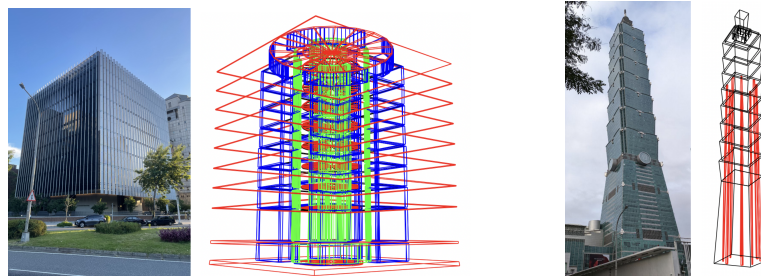


**Figure 4:** (Left) A model of CCLCH with a photo taken from the same viewing angle. Structural walls around the four corners are depicted in blue and green, while the central cylindrical hollow is highlighted in red. (Right) A model of Taipei 101 building with a photo taken from the same viewing angle. Taipei 101 building, inspired by the segmented structure of a bamboo, features eight identical nodes from 26F to 90F, with each node consisting of 8 floors. Eight  $3 \times 2\text{m}^2$  large pillars responsible for supporting the building extend from B23F to 90F, and they are filled with concrete below 62F, which are colored in red.

## 4. Results

### 4.1 Muon tomography image of CCLCH

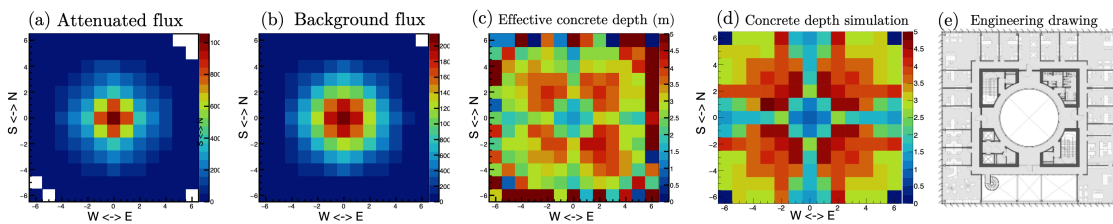


**Figure 5:** (a) Attenuated muon flux histogram collected in B1F auditorium of CCLCH. (b) Background muon flux histogram collected at roof top of CCLCH. (c) Muon tomography image showing effective concrete lengths measured by GMT<sup>2</sup>. (d) Expected muon tomography image from simulation. (e) Engineering drawing of 6F of CCLCH building for comparison. The positions of the four structural walls correspond to the areas with the thickest concrete lengths in the muon tomography image.

The muon tomography image along with attenuated and background muon flux histograms are shown in Fig. 5. Throughout a 16-day observation period for attenuated muon flux, a total of

181k muons were recorded. For the background muon flux, on the other hand, 529k muons were collected over a 25-day observation period.

In the histogram of background muon flux (Fig. 5(b)), significantly higher counts are evident at the central section. This phenomenon can be attributed to several factors: 1) The cosine-square distribution caused by the atmosphere's slant depth, resulting in the highest flux of muons arriving from the zenith. 2) The larger effective area for central bins due to GMT<sup>2</sup>'s geometry, increasing the likelihood of detecting muons with trajectories perpendicular to the detector plates (the zenith in this setup). This phenomenon remains consistent across all subsequent muon flux histograms.

From the muon tomography image (Fig. 5(c)), the cylindrical hollow in CCLCH could immediately be found at the central 9 pixels. The four corners surrounding the hollow exhibit the highest concrete lengths, while the eight bins positioned between them show less dense materials. These correspond to the structural walls at the four corners of the building and the aisles between these walls respectively (as depicted in the engineering diagram, Fig. 5(e)). The errors of effective concrete lengths in the muon tomography image are less than 10% for the central 5 × 5 pixels, and the concrete lengths closely match with the simulation results (Fig. 5(d)). On the other hand, a larger discrepancy is observed in the outer ring due to its lower statistical significance. Nevertheless, this remarkable image captured by GMT<sup>2</sup> has further motivated us to explore our next target object.

## 4.2 Muon tomography image of Taipei 101

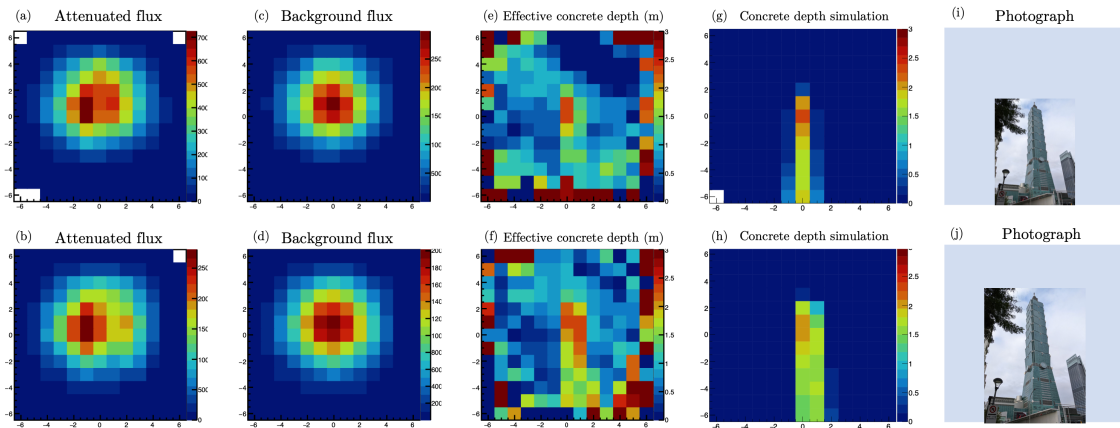


**Figure 6:** (Row 1) FOV of 90°. (Row 2) FOV of 66°. (Column 1) Attenuated muon flux observed at XinYi Elementary School. (Column 2) Background muon flux observed at an empty classroom in CCLCH. (Column 3) Muon tomography images showing effective concrete lengths measured by GMT<sup>2</sup>. (Column 4) Expected muon tomography images from simulation. (Column 5) Photographic images captured at Xinyi Elementary School using the same orientation as GMT<sup>2</sup>.

The muon tomography images of Taipei 101, along with the expected muon tomography images from simulations and corresponding photographs taken under different FOV conditions, are presented in Figure 6. We collected attenuated muon flux for 90° and 66° FOV configurations at Xinyi Elementary School over a span of 3 weeks, respectively. Approximately 200k muons were collected for an FOV of 90°, and 81k muons were collected for an FOV of 66°. At CCLCH, the background muon flux was observed for about 3 months for each FOV, resulting in a total collection of 732k and 535k background muons for FOVs of 90° and 66°, respectively.

As shown in Figure 6(e) and 6(f), the muon tomography images reveal a thinner profile of Taipei 101 at the central column for the 90° FOV and the central two columns for the 66° FOV, demonstrating the zooming capability of GMT<sup>2</sup>. In the upper section of Taipei 101, the concrete lengths are greater due to the increased slant depth as muons traverse the building. Yet, as we move to higher floors, these values gradually diminish due to the reduced floor areas beyond the 90th floor. The uncertainty of effective concrete lengths for the central 1 × 5 pixels of Taipei 101 in the 90° FOV and the central 2 × 6 pixels in the 66° FOV are less than 10%.

While a comparison of these values with the simulation results is viable, it should be noted that the simplified Taipei 101 model employed in the simulation only includes concrete and may not accurately capture the intricacies of the actual building. For a more comprehensive analysis, the simulation should incorporate steel plates, other concrete components, and various objects present within the building.

## 5. Conclusion and prospects

Muon tomography images of both CCLCH and Taipei 101 building show the ability of GMT<sup>2</sup> to conduct muon tomography. The effective concrete lengths are comparable to simulation results, which further demonstrates the feasibility of GMT<sup>2</sup> to reconstruct lengths of certain material within the FOV. With the capacity to capture 14 muons per minute from the zenith direction, GMT<sup>2</sup> enables a 10% margin of error in length estimation over a 1.5-month observation period, all within a compact device size.

As an educational program for undergraduate students, GMT<sup>2</sup> provides a valuable opportunity to develop essential skills for experimentalists, such as PCB design, signal processing, data analysis, and the physics principles underlying this field. The simplicity of operation and the straightforward physical interpretations of the results make the experience highly rewarding. In conclusion, we recommend the implementation of similar educational programs for undergraduate students interested in experimental astrophysics, as it grants them a precious opportunity to gain a comprehensive understanding of particle astrophysics.

## References

- [1] Procureur, S., Morishima, K., Kuno, M. et al., Nat Commun 14, 1144 (2023).
- [2] Nolwenn Lesparre et al., Geophys. J. Int. (2012) 190, 1008–1019
- [3] S. Cecchini and M. Spurio, arXiv:1208.1171
- [4] J.L. Autran, D. Munteanu, T. Saad Saoud, S. Moindjie. Volume 903, 21 September 2018, Pages 77-84
- [5] [https://www.abri.gov.tw/News\\_Content\\_Table.aspx?n=807&sms=9489&s=37438](https://www.abri.gov.tw/News_Content_Table.aspx?n=807&sms=9489&s=37438)